Journal: **PHILOSOPHICAL TRANSACTIONS OF THE ROYAL SOCIETY A**

Article id: **RSTA20120342**

Article Title: **Cahn–Hilliard equations incorporating elasticity: analysis and comparison to experiments**

First Author: Thomas Blesgen

Corr. Author(s): Thomas Blesgen

AUTHOR QUERIES – TO BE ANSWERED BY THE CORRESPONDING AUTHOR

As the publishing schedule is strict, please note that this might be the only stage at which you are able to thoroughly review your paper.
Please pay special attention to author names, affiliations and contact details, and figures, tables and their captions.
No changes can be made after publication.

The following queries have arisen during the typesetting of your manuscript. Please answer these queries by marking the required corrections at the appropriate point in the text.

Q1	Please provide location of the publisher in refs [21,32].	
Q2	Please update complete details for ref. [45].	

PHILOSOPHICAL TRANSACTIONS OF THE ROYAL SOCIETY A

rsta.royalsocietypublishing.org

Research

Cite this article: Blesgen T, Chenchiah IV. 2013 Cahn–Hilliard equations incorporating elasticity: analysis and comparison to experiments. Phil Trans R Soc A 20120342. http://dx.doi.org/10.1098/rsta.2012.0342

One contribution of 11 to a Theme Issue 'Entropy and convexity for nonlinear partial differential equations'.

Subject Areas:
applied mathematics, materials science, mechanics

Keywords:
Cahn–Hilliard equation, quasi-convex elastic energy density, coarsening, superalloys

Author for correspondence:
Thomas Blesgen
e-mail: blesgen@mis.mpg.de

Royal Society Publishing
Informing the science of the future

Cahn–Hilliard equations incorporating elasticity: analysis and comparison to experiments

Thomas Blesgen[1] and Isaac Vikram Chenchiah[2]

[1]Max Planck Institute for Mathematics in the Sciences, Inselstraße 22-26, 04103 Leipzig, Germany
[2]School of Mathematics, University of Bristol, University Walk, Bristol BS8 1TW, UK

We consider a generalization of the Cahn–Hilliard equation that incorporates an elastic energy density which, being quasi-convex, incorporates microstructure formation on smaller length scales. We explore the global existence of weak solutions in two and three dimensions. We compare theoretical predictions with experimental observations of coarsening in superalloys.

1. Introduction: coarsening in superalloys

Quenching a multi-component alloy produces a supersaturated metastable solid which under annealing nucleates small randomly dispersed precipitates. The precipitate morphology then evolves by diffusional mass transport as the multi-phase mixture tends to minimize its energy. During this postphase-transformation morphological evolution, the phase fractions of the matrix and precipitates remain constant. This process is known as coarsening.

Coarsening is driven by two contributions to the energy: interfacial and elastic. Given the initial small size of the precipitates, interfacial energy dominates the evolution in the beginning. However, as the particle size increases, the evolution is increasingly and eventually dominantly influenced by elastic energy arising from the difference in lattice parameters (i.e. difference in stress-free strains) between the phases. Consequently, the precipitates tend to align along specific crystallographic directions. Externally applied stresses also contribute to the energy of the system and significantly modify precipitate morphology.

Directional coarsening, also known as rafting, in which precipitates preferentially grow along certain directions, has been observed in many superalloy systems. We summarize the key experimental observations in §2.

The equilibrium state for coarsening driven purely by interfacial energy is clearly a single spherical inclusion because this is the unique geometry that minimizes the interfacial area. By contrast, the equilibrium state for coarsening driven by elastic energy alone is mathematically non-trivial and is a microstructure on an infinitesimal scale, see §3.

Apart from being of scientific interest the phenomenon of coarsening in superalloys is of technological importance because Ni-based superalloys are used in high-temperature applications, such as turbine blades, and the operating stress and temperature range for such blades is the one in which coarsening occurs. As the morphology of the material changes, so do its macroscopic properties, e.g. creep resistance.

For further information about coarsening, we recommend [1–5].

Outline of the paper. In §2, we summarize the key experimental observations pertaining to coarsening in elastic solids. In §3, we focus on a recent development, a two-scale model for elasticity-influenced coarsening first presented in [6]. We motivate the model, present some analytical results and compare the model with experimental results. We end in §4 with some mathematical reflections and questions.

We also present a generous bibliography which, while not being exhaustive, aims to be a good starting point for a unified (mathematical, mechanical and experimental) perspective on this topic. For the interested reader, we also recommend the (materials science-focused) bibliographies in [1–4] and a more mathematical bibliography in [7]. We do not review here the very many computational investigations that have been carried out, but refer the interested reader to [8–18]. Most of these are two-dimensional simulations but some are in three dimensions.

Notation. The dimension of the space is denoted by D, which could be either 2 or 3. Adopting common notation, $\cdot$ denotes the inner product in $\mathbb{R}^D$, and $:$ the inner product in $\mathbb{R}^{D\times D}$, i.e. for $A, B \in \mathbb{R}^{D\times D}$, $A : B := \mathrm{tr}(A^{\mathrm{T}}B) = \sum_{i,j=1}^{D} A_{ij}B_{ij}$.

2. Summary of key experimental observations

Here, we summarize the key experimental observations that shed light on the effect of elasticity on coarsening. First, in §2*a*, we address the morphology of the precipitates. The question as to whether elasticity changes the kinetics of coarsening has received contradictory answers in the experimental literature; we address it in §2*b*.

(a) Morphology

In the absence of external stress, the precipitates are initially spherical, becoming cuboidal and then (when the volume fraction is larger than 0.1 as is the case in most commercial Ni superalloys) coalesce to form plates whose faces are parallel to the cube directions and equi-distributed among the three possible directions. This is in keeping with the cubic symmetry of both the precipitate and the matrix.

The application of uniaxial external stress biases the microstructure, producing plates or rods oriented preferentially with respect to the cube planes. When the applied stress is parallel to [100], the precipitates form rods parallel to [100] or plates with faces parallel to (010) and (001) on the one hand, or plates with faces perpendicular to [100], on the other hand ([19] and the references therein).

In this context, as pointed out by Pollock & Argon [20] and the references therein, a simple experimental observation offers strong evidence that the morphology is decided by elastic stresses caused by differing lattice parameters between the precipitates and matrix: whether precipitates are elongated (i) perpendicular to the applied stress or (ii) parallel to the applied stress depends only on the product of the sign of the difference in lattice parameters and the sign of the applied stress.

As in experiments, rafting and plastic strain have been concurrently observed, questions have been raised as to (i) whether rafting can be explained on the basis of elasticity alone and (ii) whether purely elastic rafting can be experimentally observed. For example, Prikhodko & Ardell [19] observe only negligible purely elastic rafting in Ni–Al alloys. Arguing that for Ni–Al alloys coarsening at 900–1200 K the driving force for purely elastic rafting is negligible, they conclude that observations of rafting in Ni–Al under these conditions is owing to plastic effects.

As to (i) so very many theoretical analyses (of varying rigour) and computational investigations (using varying techniques) have shown that rafting can be explained on the basis of elasticity alone that we consider this question to be settled. (See the various review articles cited elsewhere in this paper; the most rigorous analysis we are aware of is in [21] and in §3*f*.) Issue (ii) on the other hand, can only be settled experimentally and for specific systems. We point the interested reader to [8,20,22–25]. What is clear is that a complete theory of coarsening must include plastic effects.

Finally, the particle size distribution in the presence of elastic stresses is similar (albeit broader and with lower peak height) to the one theoretically predicted for coarsening driven purely by interfacial energy [26].

(b) Kinetics

For coarsening driven only by interfacial energy, the particles remain spherical as they grow larger, and thus the radius of the particle is a natural measure of the size of the particle and the mean radius of the particles a natural length scale for the system. When elastic effects are also present, the morphology of the particles changes with time and the question arises as to how to characterize the size of the particle.

Two measures of particle size have been used in the experimental literature. The older one is mean particle size, the definition of which depends on the shape of the particle (e.g. radius for a sphere and half the side length for a cube). An alternate, more recently introduced measure is interfacial area density (i.e. interfacial area per unit volume). As there is no simple relationship between these two measures it is not possible, on the basis of published experimental findings, to convert experimental observations expressed in one of these measures into the other. Thus, we summarize the experimental findings separately.

(i) Mean particle size

Experimental investigations using this measure reveal that compressive stress reduces the coarsening rate significantly (e.g. by 20–25% in [27]). Ardell & Prikhodko [28] explain this by arguing that under uniaxial compressive stress the effective diffusivity decreases. (Under these conditions, diffusion is anisotropic and increases in the direction of the stress and decreases in the perpendicular directions.) However, it is unclear whether this can fully explain the reduction in coarsening rate, indeed there is experimental evidence [19, p. 5031] that elastic interactions among the precipitates act in synergy with applied stresses.

(ii) Interfacial area density

In experiments performed on Ni–Al alloys Lund & Voorhees [29], using this measure, found interfacial area density to grow as the cube-root of time throughout the experiment, in particular, even after very long times. This is significant in that the one-third power law is well established for coarsening driven purely by interfacial energy reduction and scaling argument lead us to expect the same also when elastic effects are present. Moreover, the coarsening rate constant depends on volume fraction as theoretically predicted. Finally, interfacial area density seems to provide a length scale for the system which is independent of morphology or distribution of the precipitates; figure 1 illustrates this.

It is clear that conceptually the interfacial energy density is superior to the *ad hoc* notions of mean particle size used until recently in the experimental literature. That, under this measure, the

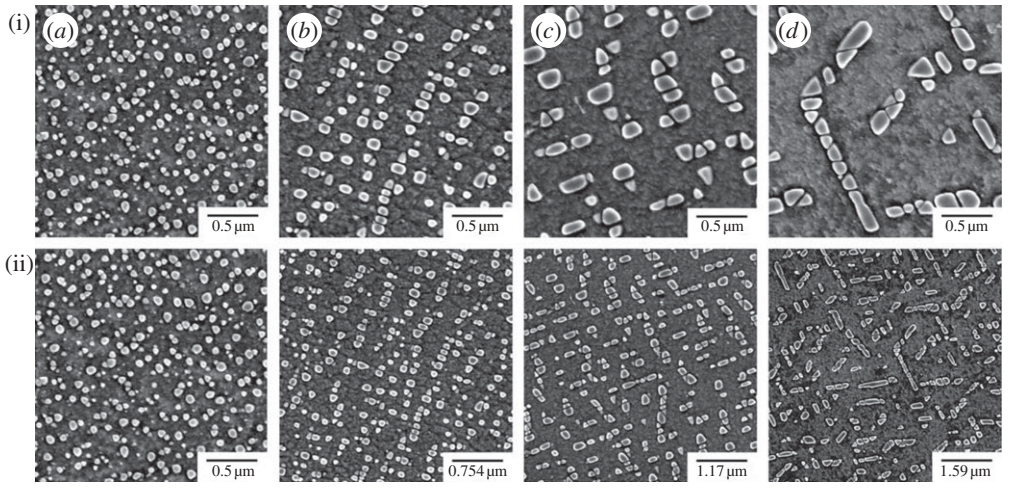

Figure 1. Coarsening in a Ni–Al alloy with 14.5% volume fraction of precipitates after (*a*) 30 min, (*b*) 93 min, (*c*) 589 min and (*d*) 1097 min. The magnification is constant on (i) but has been scaled by the interfacial area density for (ii) [29].

one-third power law and morphology-invariant length scale have been experimentally observed leads to a compelling case for the use of this measure to characterize coarsening.

3. A recent two-scale approach to modelling coarsening

(a) Historical background

The focus of this paper lies on extending the elastic Cahn–Hilliard (CH) equation to incorporate elasticity with microstructure. To give a better understanding of the underlying concepts, we start with a review of the history of this equation and related models.

The original CH model was introduced in 1958, [30], to explain spinodal decomposition in binary alloys under isothermal conditions for a temperature θ below the critical temperature θ_c of the solid. The derivation builds on the Landau–Ginzburg theory, and an (conserved) order parameter χ is introduced to describe the spatial distribution of the phases. The phases themselves are identified as minimizers of the free energy. In the bulk phase, neglecting elastic effects for the moment, they thus minimize $\int_\Omega \psi \, \mathrm{d}x$ with a double-well potential ψ (originally $\psi(\chi) := 0.25(\chi^2 - 1)^2$, but see (3.2)). As the interfaces diffuse, 'mushy regions' occur. The concepts behind the classical CH equation are well explained in the survey article [31].

The early mathematical treatment of the classical 1958 model failed as the analysis was based on linearization which changed the fundamental properties of the solution and lead to unphysical behavior. In the 1980s, the analysis was finally put on a solid basis.

In due course, the original CH model was extended in many directions. We name here the generalization to multiple phases [32]; to non-isothermal settings [33,34]; to concentration-dependent mobilities [35]; the incorporation of convective [36] and viscous effects [37,38]; the coupling to the Navier–Stokes equations [39,40] and the derivation of a general CH/Allen–Cahn model [41]. The sharp interface limit of the CH model (and their extensions) is also well understood [42–44]. Besides a classification of the different models, this resulted in a better understanding of surface tension and the role of the Gibbs–Thomson law [45]. A currently very active area of research is the investigation of statistical phenomena in nucleation and phase change models. For the CH equation, Brownian motion was first considered in [46]. Fluctuations of the interfaces of the new model were studied for the first time in [47].

In this article, we concentrate on extending the Cahn–Larché model. The system with linear elasticity was mainly studied in [48–51]. Finally, up-to-date numerics and references to computational methods for the CH model can be found in [52].

(b) Motivation

A successful model of coarsening should account for both interfacial and elastic contributions to the energy. Unfortunately, rigorous analysis of such energy functionals is beyond the capabilities of current mathematical tools. Indeed, with only a few exceptions, this is true even for static problems.

In an effort to advance the mathematical understanding of coarsening in [6], we put forth a model that aims to account for both interfacial and elastic energies but nevertheless holds forth hope of being analytically tractable. It achieves this by incorporating these energies on different scales. This is motivated by the intuition that interfacial energy sets the length scale of the morphology but elasticity decides its geometric features (patterns). Thus, it is natural to consider these energetic contributions on different spacial scales.

Thus our model, which we introduce in detail in §3*c*, is two-scale (in space). On the larger length scale—*which is larger than the morphological length scale*—both interfacial and elastic energies are present but, precisely because we are on a length scale larger than the morphological length scale, these energies see only a homogenized morphology.

At the lower length scale, which is the morphological length scale, we neglect interfacial energy. Then the passage from this length scale to the larger length scale is achieved by relaxing the elastic energy; this is the topic of §3*d*. The key point to note here is that by neglecting interfacial energy, we obtain a problem that is tractable, indeed that has been rigorously solved [53].

Thus, the elastic energy on the larger length scale sees not a morphology but a microstructure, that is to say a scale-free morphology, or in other words, only the geometry (pattern) of the morphology. Such a homogenized perspective can be expected to capture the elastic contributions which are long range but do they adequately treat the interfacial energy? This question arises because the interfacial energy in our model, being on the larger length scale, is associated not with the physical interfaces in the morphology but with variations in the homogenized volume fraction. Preliminary computational investigations in [6] appear to show that, yes, they do. It is intriguing to ask whether an analysis can rigorously show this.

Next in §3*e*, we turn to the question as to whether the model is analytically tractable. The existence and uniqueness theorems that we present are only a start but are promising. (In §4, we comment on the obstacles that must be overcome to extend these results.)

Finally, in §3*f* we compare the microstructures predicted by our model with the morphologies observed in experiments.

(c) The model

The system that we investigate comprises the evolution equations (3.1) together with the entropic free energy density (3.2) and the (relaxed) elastic energy density (3.3). The evolution equations are

$$\partial_t \chi = \operatorname{div}(L\nabla\mu), \tag{3.1a}$$

$$\mu = -\gamma\triangle\chi + \psi'(\chi) + \partial_\chi \hat{W}(\chi, \varepsilon(\mathbf{u})) \tag{3.1b}$$

and

$$0 = \operatorname{div}(\partial_\varepsilon \hat{W}(\chi, \varepsilon(\mathbf{u}))) \tag{3.1c}$$

to be solved in a space–time cylinder $\Omega_S := \Omega \times (0, S)$, where $S > 0$ is a stop time and $\Omega \subset \mathbb{R}^D$ is a bounded domain with Lipschitz boundary containing the solid. Here, $\gamma > 0$ is the (isotropic) surface energy; L, assumed to be positive-definite, is the mobility tensor; and $\chi : \Omega_S \to [0, 1]$ is the volume fraction of one phase of the solid.

Equations (3.1) are frequently referred to as *Cahn–Larché system* [54]; (3.1*a*) and (3.1*b*) alone (without elasticity) constitute the classical *CH equation* [30]. The model is phenomenological in that Onsager's law $J = -L\nabla\mu$ [55,56] is assumed for the mass flux which may be invalid far away from thermodynamic equilibrium and in that heuristic assumptions are made for the free energy and for the interface.

The entropic free energy density ψ is

$$\psi(\chi) = k_B\theta(\chi_1 \ln \chi_1 + \chi_2 \ln \chi_2) + \frac{\theta_c}{2}\chi_1\chi_2, \tag{3.2}$$

where, for convenience, $\chi_1 := \chi$ and $\chi_2 := (1 - \chi)$. Here, k_B is the Boltzmann constant, $\theta > 0$ the (constant) temperature, and θ_c the critical temperature where spinodal decomposition starts.

The elastic energy density $\hat{W}$ is the subject of the following section.

(d) The elastic energy density

We assume that each phase is linearly elastic:

$$W_i(\varepsilon) := \frac{1}{2}\alpha_i(\varepsilon - \varepsilon_i^T) : (\varepsilon - \varepsilon_i^T) + w_i, \quad i = 1, 2.$$

Here, ε_i^T is the stress-free strain of phase i and $w_i \in \mathbb{R}_+$ is its minimum energy density. However, in contrast to preceding work, instead of postulating the energy density of a mixture of the two phases, we derive it rigorously. Our reasoning is as follows.

We interpret the order parameter $\chi(x) \in [0, 1]$ as prescribing the volume fractions of the two phases at $x \in \Omega$, i.e. in a ball $B_r(x) \subset \Omega$. (This assumes that the regions occupied by each of the two phases in $B_r(x)$ are measurable.) Thus, if $\tilde{\chi}_1 \equiv \tilde{\chi}$, $\tilde{\chi}_2 = 1 - \tilde{\chi}$ are the characteristic functions of the two phases on the microscale, we have $\tilde{\chi}_i \in BV(B_r(x); \{0, 1\})$ and

$$\chi_i(x) = \langle\tilde{\chi}_i\rangle := \frac{1}{|B_r(x)|}\int_{B_r(x)} \tilde{\chi}_i(y)\,\mathrm{d}y, \quad i = 1, 2,$$

where $|E|$ is the D-dimensional Lebesgue measure of a set E. In the absence of microstructural surface energy, the elastic energy of this ball for a microscale displacement $\tilde{\mathbf{u}}$ is

$$\int_{B_r(x)} \tilde{\chi}_1 W_1(\varepsilon(\tilde{\mathbf{u}})) + \tilde{\chi}_2 W_2(\varepsilon(\tilde{\mathbf{u}}))\,\mathrm{d}y.$$

Next, we postulate that the system selects $\tilde{\chi}$ and $\tilde{\mathbf{u}}$ to minimize the microscopic elastic energy. (Thus, the deformations adopt instantaneously to diffusion-induced changes in concentration. In other words, elastic time scales are much shorter than diffusion time scales.) This reasoning leads us to conclude that the macroscopic elastic energy density is

$$\hat{W}(\chi, \varepsilon) := \inf_{\langle\tilde{\chi}\rangle = \chi} \inf_{\tilde{\mathbf{u}}_{|\partial B_r} = \varepsilon x} \frac{1}{|B_r(x)|}\int_{B_r(x)} \tilde{\chi}_1 W_1(\varepsilon(\tilde{\mathbf{u}})) + \tilde{\chi}_2 W_2(\varepsilon(\tilde{\mathbf{u}}))\,\mathrm{d}x. \tag{3.3}$$

The considerations leading to (3.3) are purely heuristic. The microscopic and macroscopic length scales are coupled through the constraint $\langle\tilde{\chi}\rangle = \chi$ only, i.e. no additional information on the local geometry of the domain is passed to the lamination microstructure, nor are there conditions on the time behaviour of $\tilde{\chi}$, e.g. a connection between dynamical effects such as momentum between χ and $\tilde{\chi}$. The minimization of the elastic energy on the microscale reflects the assumption of mechanical equilibrium on the macroscopic scale as expressed by (3.1*c*).

The definition (3.3) of $\hat{W}$ is in fact independent of r, e.g. [57]. Mathematically, the infimum over $\tilde{\chi}$ in (3.3) is the result of relaxation subjected to prescribed volume fractions (e.g. [58]).

The (analytical) computation of $\hat{W}$ is non-trivial for dimensions larger than one. Explicit (albeit involved) expressions were derived in [53]. We reproduce them here.

(i) In two dimensions

In two dimensions, $\hat{W}$ is completely known, see (3.7).

With $T\colon \mathbb{R}^{2\times 2}_{\mathrm{sym}} \to \mathbb{R}^{2\times 2}_{\mathrm{sym}}$ being the linear operator defined by

$$T\varepsilon := \varepsilon - \mathrm{tr}(\varepsilon)\mathrm{I}, \tag{3.4a}$$

let $\gamma_i > 0$ be the reciprocal of the largest eigenvalue of $\alpha_i^{-1/2} T \alpha_i^{-1/2}$ and

$$\gamma^* := \min\{\gamma_1, \gamma_2\}. \tag{3.4b}$$

Next, for $\beta \in [0, \gamma^\star]$, let

$$\left.\begin{aligned} \alpha(\beta,\chi) &:= \chi_2\alpha_1 + \chi_1\alpha_2 - \beta T, \\ \varphi(\beta,\chi,\varepsilon) &:= -\det(\alpha^{-1}(\beta^*,\chi)((\alpha_1-\alpha_2)\varepsilon + (\alpha_2\varepsilon_2^{\mathrm{T}} - \alpha_1\varepsilon_1^{\mathrm{T}}))) \end{aligned}\right\}$$

$$\text{and} \qquad [0,\gamma^*] \ni \beta^*(\chi,\varepsilon) := \begin{cases} 0 & \text{if } \varphi(\cdot,\chi,\varepsilon) \equiv 0 \quad \text{(Regime 0)}, \\ 0 & \text{if } \varphi(0,\chi,\varepsilon) > 0 \quad \text{(Regime I)}, \\ \beta_{II}(\chi,\varepsilon) & \text{if } \varphi(0,\chi,\varepsilon) \le 0 \text{ and } \varphi(\gamma^*,\chi,\varepsilon) \ge 0 \quad \text{(Regime II)}, \\ \gamma^* & \text{if } \varphi(\gamma^*,\chi,\varepsilon) < 0 \quad \text{(Regime III)}, \end{cases} \tag{3.5}$$

where $\beta_{II}(\chi,\varepsilon)$ is the unique solution of $\varphi(\cdot,\chi,\varepsilon) = 0$. (It can be shown that this is well defined and the four regimes are mutually exclusive.) Finally, let

$$\left.\begin{aligned} \varepsilon_1^*(\beta^*,\chi,\varepsilon) &:= \alpha^{-1}(\beta^*,\chi)((\alpha_2-\beta^*T)\varepsilon - \chi_2(\alpha_2\varepsilon_2^{\mathrm{T}} - \alpha_1\varepsilon_1^{\mathrm{T}})) \\ \text{and} \qquad \varepsilon_2^*(\beta^*,\chi,\varepsilon) &:= \alpha^{-1}(\beta^*,\chi)((\alpha_1-\beta^*T)\varepsilon + \chi_1(\alpha_2\varepsilon_2^{\mathrm{T}} - \alpha_1\varepsilon_1^{\mathrm{T}})). \end{aligned}\right\} \tag{3.6}$$

Then,

$$\hat{W}(\chi,\varepsilon) = \chi_1 W_1(\varepsilon_1^*) + \chi_2 W_2(\varepsilon_2^*) + \beta^*\chi_1\chi_2 \det(\varepsilon_2^* - \varepsilon_1^*). \tag{3.7}$$

Remark 3.1. The different regimes are associated with different microstructures:

0. Any arrangement of phases is possible (because the phases are elastically indistinguishable in that the energy does not depend on the microstructure).
I. Two rank-1 laminates are possible.
II. The microstructure is necessarily a rank-1 laminate.
III. Two rank-two laminates are possible but rank-1 laminates are not.

Figure 2 illustrates rank-1 and rank-2 laminates.

(ii) In three dimensions

In three dimensions, $\hat{W}$ is completely known in the following situations: (i) both elastic moduli are isotropic or (ii) the elastic moduli are well-ordered (i.e. $\alpha_1 \le \alpha_2$ in the sense of quadratic forms) and the smaller elastic modulus is isotropic. Moreover, $\hat{W}$ is almost completely known when the elastic moduli possess cubic symmetry. However, the most-explicit expression available for $\hat{W}$ is cumbersome to write down. Instead, here we present a less explicit expression and refer to [53] for details:

$$\hat{W}(\chi,\varepsilon) \ge \max_{\beta\in S(\alpha_1)\cap S(\alpha_2)} \max_{R\in \mathrm{SO}(3)} \min_{\substack{\varepsilon_1,\varepsilon_2\in\mathbb{R}^{3\times 3}_{\mathrm{sym}} \\ \chi_1\varepsilon_1+\chi_2\varepsilon_2=\varepsilon}} \chi_1 W_1(\varepsilon_1) + \chi_2 W_2(\varepsilon_2) + \chi_1\chi_2\beta\cdot\Phi(R^{\mathrm{T}}(\varepsilon_2-\varepsilon_1)R), \tag{3.8}$$

where SO(3) is the special orthogonal group in $\mathbb{R}^3$, $\Phi\colon \mathbb{R}^{3\times 3}_{\mathrm{sym}} \to \mathbb{R}^3$ is defined by

$$\Phi(\varepsilon) = \begin{pmatrix} \varepsilon_{23}^2 - \varepsilon_{22}\varepsilon_{33} \\ \varepsilon_{31}^2 - \varepsilon_{33}\varepsilon_{11} \\ \varepsilon_{12}^2 - \varepsilon_{11}\varepsilon_{22} \end{pmatrix} \tag{3.9}$$

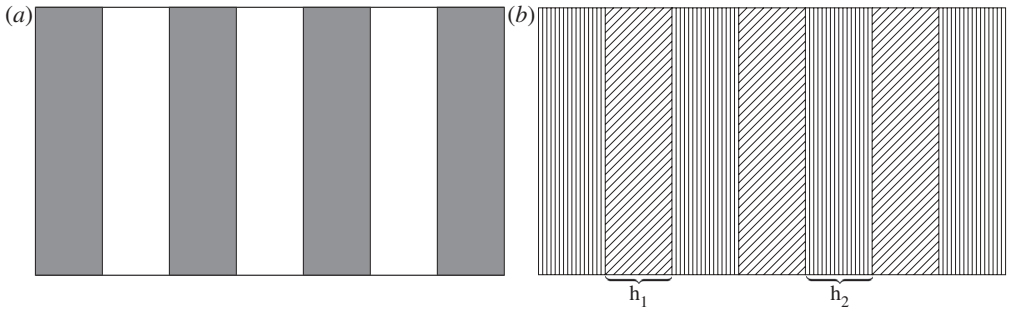

Figure 2. Two-phase rank-1 and rank-2 laminates in two dimensions. The strain is (globally) constant in each shaded region. (*a*) A rank-1 laminate. In this illustration, the volume fraction of each phase is 0.5. (*b*) A rank-2 laminate. Note the separation in length scale between the layers.

and for a cubic elastic modulus α with Lamé modulus ℓ, diagonal shear modulus μ and off-diagonal shear modulus η, with $m = \min(\mu, \eta)$,

$$S(\alpha) := \{\beta \in [0,\infty)^3 \mid 2\beta_1\beta_2\beta_3 - (\ell + 2m)(\beta_1^2 + \beta_2^2 + \beta_3^2) + 2\ell(\beta_1\beta_2 + \beta_2\beta_3 + \beta_3\beta_1) - 4\ell m(\beta_1 + \beta_2 + \beta_3) + 12\ell m^2 + 8m^3 \geq 0\}.$$

On the basis of the optimal value of β in (3.8) five regimes arise. The microstructures associated with the first four are as in two dimensions (remark 3.1) and in this case the inequality in (3.8) is in fact an equality.

In the new regime, Regime IV, which occurs when the optimal β equals $\gamma^*(1,1,1)$ (cf. (3.4*b*)), it is possible that the inequality in (3.8) is strict. However, it is an equality if either (i) both α_1 and α_2 are isotropic or (ii) $\alpha_1 \leq \alpha_2$ and α_1 is isotropic. In this case the microstructure could be a rank-2 or rank-3 laminate but not a rank-1 laminate.

Of these five regimes, Regimes 0 and IV are analytically the simplest and we have a simpler expression for $\hat{W}$:

$$\hat{W}(\chi, \varepsilon) = \chi_1 W_1(\varepsilon_1^*) + \chi_2 W_2(\varepsilon_2^*) - 2\chi_1\chi_2\beta^* e \cdot \Phi(\varepsilon_2^* - \varepsilon_1^*), \tag{3.10}$$

where β^* is 0 in Regime 0 and γ^* in Regime IV (cf. (3.4*b*)), the optimal strains ε_1^* and ε_2^* are given by (3.6) and $e = (1,1,1)$. In particular,

$$e \cdot \Phi(\varepsilon) = \frac{1}{2} T\varepsilon : \varepsilon \tag{3.11}$$

with T as in (3.4*a*).

This completes our description of the model. Next, we explore existence and uniqueness of solutions.

(e) Analysis

(i) Two dimensions

The two-dimensional Cahn–Larché system was studied in [6]. The main result was an existence theorem.

Theorem 3.2 ($D = 2$). *At each time let the system be either globally in Regime 0 or globally in Regime III. Moreover α_i and T commute. Then, there exists a weak solution $(\chi, \mu, \mathbf{u})$ to the Cahn–Larché system with microstructure (3.1), (3.2) and (3.7) such that*

(*i*) $\chi \in C^{0,1/4}([0,S]; L^2(\Omega))$,
(*ii*) $\partial_t \chi \in L^2([0,S]; (H^1(\Omega))')$,

(*iii*) $\mathbf{u} \in L^\infty([0,S];H^1(\Omega;\mathbb{R}^D))$,
(*iv*) $\mu \in L^2([0,S];H^1(\Omega))$,
(*v*) $\ln(\chi), \ln(1-\chi) \in L^1(\Omega_S)$ *and in particular* $\chi \in (0,1)$ *a.e. in* Ω.

Our proof critically relied on the following remark [50], see also [59].

Remark 3.3. $\hat{W}$ possesses the following properties:

(A1) $\hat{W} \in C^1([0,1] \times \mathbb{R}^{D\times D}_{\mathrm{sym}};\mathbb{R})$.
(A2) $\partial_\varepsilon \hat{W}(\chi,\cdot)$ is strongly monotone uniformly in χ, i.e. there exists a constant $C_1 > 0$ independent of χ such that for all $\varepsilon_a, \varepsilon_b \in \mathbb{R}^{D\times D}_{\mathrm{sym}}$,

$$(\partial_\varepsilon \hat{W}(\chi,\varepsilon_a) - \partial_\varepsilon \hat{W}(\chi,\varepsilon_b)) : (\varepsilon_a - \varepsilon_b) \geq C_1 |\varepsilon_a - \varepsilon_b|^2.$$

(A3) There exists a constant $C_2 > 0$ such that for all $\chi \in \mathbb{R}, \varepsilon \in \mathbb{R}^{D\times D}_{\mathrm{sym}}$,

$$|\hat{W}(\chi,\varepsilon)| \leq C_2(|\chi|^2 + |\varepsilon|^2 + 1),$$
$$|\partial_\chi \hat{W}(\chi,\varepsilon)| \leq C_2(|\chi|^2 + |\varepsilon|^2 + 1)$$
and
$$|\partial_\varepsilon \hat{W}(\chi,\varepsilon)| \leq C_2(|\chi| + |\varepsilon| + 1).$$

As for uniqueness of the weak solutions, only the following weak result is known.

Theorem 3.4 ($D = 2$). *Let the two phases have identical elastic moduli, $\alpha_1 = \alpha_2$. Then the weak solution $(\chi,\mu,\mathbf{u})$ of (3.1), (3.2) and (3.7) is unique in the spaces stated in theorem 3.2.*

(ii) Three dimensions

We now present the following new existence and uniqueness result that extends theorems 3.2 and 3.4 to three dimensions.

Theorem 3.5 ($D = 3$). *Let either (i) both elastic moduli be isotropic or (ii) the elastic moduli be well-ordered, the larger elastic modulus commute with T and the smaller elastic modulus be isotropic. Moreover, at each time let the system be either globally in Regime 0 or globally in Regime IV. Then there exists a weak solution $(\chi,\mu,\mathbf{u})$ to (3.1), (3.2) and (3.10) with the regularity properties stated in theorem 3.2. If additionally $\alpha_1 = \alpha_2$, then $(\chi,\mu,\mathbf{u})$ is unique in the spaces stated in theorem 3.2.*

The proof of theorem 3.5 has the same structure as the proof of theorem 3.2. The first and critical step is to verify that $\hat{W}$ has the properties in remark 3.3.

Lemma 3.6 ($D = 3$). *Let either (i) both elastic moduli be isotropic or (ii) the elastic moduli be well-ordered, the larger elastic modulus commute with T and the smaller elastic modulus be isotropic. Then, in Regime 0 and in Regime IV, $\hat{W}$ possesses the properties (A1)–(A3) of remark 3.3.*

Proof. (i) It can be directly verified that $\hat{W}$ is continuously differentiable as needed for (A1).
(ii) *Proof of* $(A3)_1$. As $\beta^* = 0$ or $\beta^* = \gamma^*$ and because γ^* depends only on α_1 and α_2,

$$|\beta^*| \leq c. \tag{3.12}$$

Here (and henceforth), c denotes a generic non-negative constant independent of χ and ε. From (3.10) and (3.12),

$$|\varepsilon_i^*(\beta^*,\chi,\varepsilon)| \leq c(|\chi| + |\varepsilon| + 1), \quad i = 1,2.$$

Now, as

$$|W_i(\varepsilon)| \leq c(|\varepsilon|^2 + 1),$$

we find by straightforward computations because $|\chi|^2 \le 1$ (we only need to consider $-1 \le \chi \le +1$, for $\chi \notin [-1,+1]$ the extension of $\hat{W}$ given in [6] then satisfies the growth conditions),

$$\begin{aligned}|\hat{W}(\chi,\varepsilon)| &= |\chi_1 W_1(\varepsilon_1^*) + \chi_2 W_2(\varepsilon_2^*) - 2\mu\chi_1\chi_2 e\cdot\Phi(\varepsilon_2^*-\varepsilon_1^*)|\\ &\le c|\chi|(|\varepsilon_1^*|^2+|\varepsilon_2^*|^2+1) + c(|\varepsilon_1^*|^2+|\varepsilon_2^*|^2)|\chi|^2\\ &\le c(|\chi|^2+|\varepsilon|^2+1).\end{aligned}$$

(iii) *Proof of* $(A3)_2$, $(A3)_3$. The first fundamental observation is that T, α and α_i commute either by assumption or because of isotropy. Let $\alpha(\beta,\chi)$ be as defined in (3.5) and $\Delta\varepsilon^* := \varepsilon_2^*(\beta^*,\chi,\varepsilon) - \varepsilon_1^*(\beta^*,\chi,\varepsilon)$ (cf. (3.6)). The following identities can be proved (for Regimes 0 and IV in three dimensions) by direct inspection:

$$\frac{\mathrm{d}\varepsilon_1^*}{\mathrm{d}\chi} = (\mathrm{I} + \chi_2\alpha^{-1}(\alpha_2-\alpha_1))\Delta\varepsilon^* \tag{3.13a}$$

and

$$\frac{\mathrm{d}\varepsilon_2^*}{\mathrm{d}\chi} = (\mathrm{I} - \chi_1\alpha^{-1}(\alpha_2-\alpha_1))\Delta\varepsilon^*, \tag{3.13b}$$

$$\frac{\mathrm{d}\varepsilon_1^*}{\mathrm{d}\varepsilon} = \alpha^{-1}(\alpha_2-\beta^*T),$$

$$\frac{\mathrm{d}\varepsilon_2^*}{\mathrm{d}\varepsilon} = \alpha^{-1}(\alpha_1-\beta^*T),$$

and

$$\frac{\mathrm{d}\Delta\varepsilon^*}{\mathrm{d}\varepsilon} = \alpha^{-1}(\alpha_1-\alpha_2),$$

$$\frac{\mathrm{d}W_1(\varepsilon_1^*)}{\mathrm{d}\chi} = \alpha_1(\varepsilon_1^*-\varepsilon_1^{\mathrm{T}}) : (\mathrm{I} + \chi_2\alpha^{-1}(\alpha_2-\alpha_1))\Delta\varepsilon^* \tag{3.14a}$$

and

$$\frac{\mathrm{d}W_2(\varepsilon_1^*)}{\mathrm{d}\chi} = \alpha_2(\varepsilon_2^*-\varepsilon_2^{\mathrm{T}}) : (\mathrm{I} - \chi_1\alpha^{-1}(\alpha_2-\alpha_1))\Delta\varepsilon^*, \tag{3.14b}$$

$$\frac{\mathrm{d}W_1(\varepsilon_1^*)}{\mathrm{d}\varepsilon} = (\alpha_2-\beta^*T)\alpha^{-1}\alpha_1(\varepsilon_1^*-\varepsilon_1^{\mathrm{T}})$$

and

$$\frac{\mathrm{d}W_2(\varepsilon_2^*)}{\mathrm{d}\varepsilon} = (\alpha_1-\beta^*T)\alpha^{-1}\alpha_2(\varepsilon_1^*-\varepsilon_1^{\mathrm{T}}).$$

As $T\varepsilon : \varepsilon' = e\cdot\Phi'(\varepsilon)$,

$$\begin{aligned}-e\cdot\frac{\mathrm{d}\Phi(\varepsilon_2^*-\varepsilon_1^*)}{\mathrm{d}\chi} &= -T(\varepsilon_2^*-\varepsilon_1^*) : \frac{\mathrm{d}(\varepsilon_2^*-\varepsilon_1^*)}{\mathrm{d}\chi}\\ &= T\alpha^{-1}(\alpha_2-\alpha_1)(\varepsilon_2^*-\varepsilon_1^*) : (\varepsilon_2^*-\varepsilon_1^*),\end{aligned}$$

where (3.13) was used. Similarly, for $f \in \mathbb{R}^{3\times3}_{\mathrm{sym}}$,

$$\begin{aligned}e\cdot\frac{\mathrm{d}\Phi(\varepsilon_2^*-\varepsilon_1^*)}{\mathrm{d}\varepsilon} : f &= T(\varepsilon_2^*-\varepsilon_1^*) : \alpha^{-1}(\alpha_1-\alpha_2)f\\ &= (\alpha_1-\alpha_2)\alpha^{-1}T(\varepsilon_2^*-\varepsilon_1^*) : f.\end{aligned}$$

These results put us in the position to compute the main equalities

$$\begin{aligned}\frac{\mathrm{d}\hat{W}}{\mathrm{d}\chi}(\chi,\varepsilon) &= \frac{\mathrm{d}}{\mathrm{d}\chi}(\chi_1^* W_1(\varepsilon_1^*) + \chi_2 W_2(\varepsilon_2^*) - 2\mu\chi_1\chi_2\beta^* e\cdot\Phi(\Delta\varepsilon^*))\\ &= \bar{\sigma}^* : \Delta\varepsilon^* - \chi_1\chi_2\Delta\sigma^* : \alpha^{-1}(\alpha_2-\alpha_1)(\Delta\varepsilon^*) + W_1(\varepsilon_1^*) - W_2(\varepsilon_2^*)\\ &\quad - 2\mu(\chi_2-\chi_1)\beta^* e\cdot\Phi(\Delta\varepsilon^*) + 2\chi_1\chi_2\beta^* T\alpha^{-1}(\alpha_2-\alpha_1)\Delta\varepsilon^* : \Delta\varepsilon^*\end{aligned} \tag{3.15}$$

and

$$\frac{\mathrm{d}\hat{W}}{\mathrm{d}\varepsilon}(\chi,\varepsilon)=\chi_1(\alpha_2-\beta^*T)\alpha^{-1}\alpha_1(\varepsilon_1^*-\varepsilon_1^{\mathrm{T}})+\chi_2(\alpha_1-\beta^*T)\alpha^{-1}\alpha_2(\varepsilon_2^*-\varepsilon_2^{\mathrm{T}})$$
$$+2\chi_1\chi_2\beta^*T\alpha^{-1}(\alpha_2-\alpha_1)\Delta\varepsilon^*, \tag{3.16}$$

where we used the shorthand notation $\sigma_i^*:=\alpha_i(\varepsilon_i^*-\varepsilon_i^{\mathrm{T}})$, $\bar{\sigma}^*:=\chi_1\sigma_1^*+\chi_2\sigma_2^*$ and $\Delta\sigma^*:=\sigma_2^*-\sigma_1^*$. The proof of $(A3)_2$ can then be carried out as in two dimensions, estimating consecutively all the terms in (3.15), (3.16). We just mention

$$|\bar{\sigma}^*(\chi,\varepsilon)|=\left|\sum_{i=1}^{2}\chi_i\alpha_i(\varepsilon_i^*-\varepsilon_i^{\mathrm{T}})\right|\le c(|\chi|+|\varepsilon|+1),$$

$$|\Delta\varepsilon^*(\chi,\varepsilon)|=|\varepsilon_2^*-\varepsilon_1^*|\le c(|\chi|+|\varepsilon|+1)$$

and

$$|\beta^*e\cdot\Phi(\Delta\varepsilon^*)|\le\gamma^*|e\cdot\Phi(\Delta\varepsilon^*)|=\frac{\gamma^*}{2}T\Delta\varepsilon^*:\Delta\varepsilon^*$$
$$=\frac{\gamma^*}{2}(\Delta\varepsilon^*-\mathrm{tr}(\Delta\varepsilon^*)\mathrm{I}):\Delta\varepsilon^*\le c|\Delta\varepsilon^*|^2\le c(|\chi|^2+|\varepsilon|^2+1).$$

This proves $(A3)_2$. The proof of $(A3)_3$ estimates the terms on the right-hand side of (3.16), and we leave out the (simple) details.

(iv) *Proof of* (*A2*). Let ε_a, $\varepsilon_b\in\mathbb{R}^{3\times3}_{\mathrm{sym}}$. The monotonicity of $\partial_\varepsilon\hat{W}(\chi,\cdot)$ crucially depends on the expressions

$$(\varepsilon_1^*(\varepsilon_a)-\varepsilon_1^*(\varepsilon_b)):(\varepsilon_a-\varepsilon_b)=\alpha^{-1}(\alpha_2-\beta^*T)(\varepsilon_a-\varepsilon_b):(\varepsilon_a-\varepsilon_b) \tag{3.17a}$$

and

$$(\varepsilon_2^*(\varepsilon_a)-\varepsilon_2^*(\varepsilon_b)):(\varepsilon_a-\varepsilon_b)=\alpha^{-1}(\alpha_1-\beta^*T)(\varepsilon_a-\varepsilon_b):(\varepsilon_a-\varepsilon_b) \tag{3.17b}$$

which follow from (3.6). We use (3.17) in the explicit representation (3.16) and note further that $(\alpha_i-\beta^*T)$, $i=1,2$, are positive-definite and that α is fixed as χ is fixed and β^* is constant in the two considered regimes. The explicit representation (3.16) then yields (A2). ■

Proof of theorem 3.5. Based on Lemma 3.6, the proof of existence of weak solutions with the stated regularity properties follows the key steps of the proof of the two-dimensional version of Theorem 3.2 in [6].

The proof of uniqueness for $\alpha_1=\alpha_2$ relies on Gronwall's and Korn's inequality and exploits the fact that for two pairs of solutions $(\chi^A,\mu^A,\mathbf{u}^A)$ and $(\chi^B,\mu^B,\mathbf{u}^B)$,

$$\beta^*(\chi^B,\varepsilon^B)=\beta^*(\chi^A,\varepsilon^A),\quad \varepsilon_i^*(\chi^B,\varepsilon^B)=\varepsilon_i^*(\chi^A,\varepsilon^A),\quad i=1,2$$

in the two considered regimes 0 and IV. Consequently, the critical term

$$\int_{\Omega\times(0,t_0)}(\partial_\chi\hat{W}(\chi^B,\varepsilon^B)-\partial_\chi\hat{W}(\chi^B,\varepsilon^A))(\chi^B-\chi^A)\mathrm{d}(x,t)$$

vanishes identically. The proof then follows exactly as in two dimensions. ■

In §4, we comment on the obstacles that prevent us from extending these results to the other regimes, and when the regimes are spatially varying. Before that we compare the predictions of this model with experiments.

(f) Experimental assessment

Here, we present a preliminary, qualitative comparison between the microstructures predicted by our model and the morphology observed in experiments (see also [21]). We are unable to quantitatively compare our predictions with experimental results because we do not know the elastic constants for most of the materials experimented on. (However, these can be estimated or computed by *ab initio* methods.)

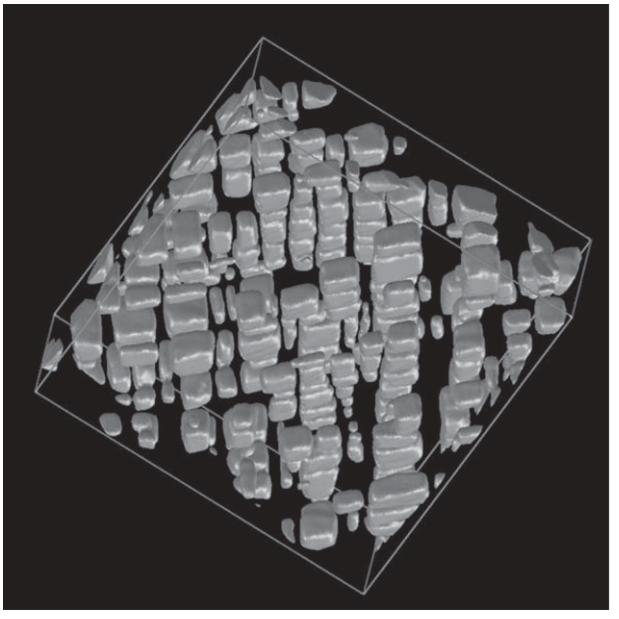

Figure 3. A characteristic portion of the three-dimensional rendered microstructure observed by Lund & Voorhees [26]. The frame around the microstructural volume is $7.5 \times 7.5 \times 3.6\ \mu$m. Precipitates truncated by the top or bottom of the experimental volume have been removed.

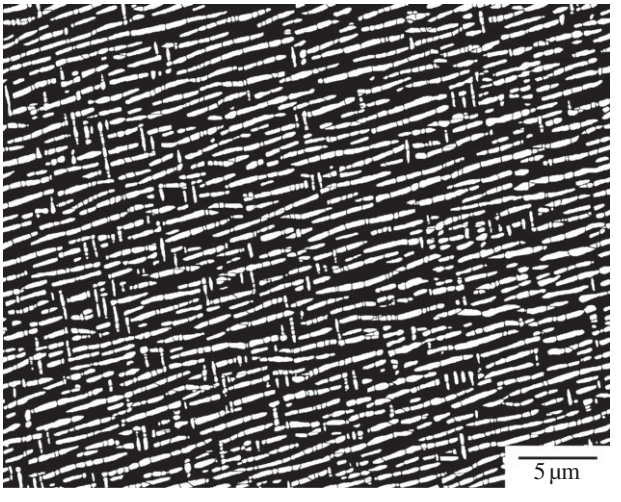

Figure 4. Ni-Al alloy with volume fraction 24.8% of precipitates after 2296 min at 1173 K (thresholded and binaried image), [29].

The first step is to relate the (scale-free) microstructures of our analysis to expected morphologies. This is easy to do (figure 2); the natural identification in three dimensions is to identify rank-1 laminates with plate-like precipitates, rank-2 laminates with rod-like precipitates and rank-three laminates with cuboidal precipitates. With this identification there is considerable experimental evidence for these microstructures. We mention here only two striking observations.

In a remarkable experiment, Lund & Voorhees have rendered actual three-dimensional microstructures by sectioning followed by reconstruction [26]. Their observation that 'particles tend to align with each other in parallel two-dimensional sheets' is consistent with laminates.

In particular, in figure 3 one can see the cuboidal precipitates aligned as in a rank-3 laminate. The close-spaced precipitates might be in the process of evolving to rods (i.e. rank-2 laminates) or sheets (i.e. rank-1 laminates).

Another observation of Lund & Voorhees [29] on a Ni–Al alloy might be evidence of the unique rank-1 laminate of Regime II (cf. remark 3.1). As can be seen in figure 4, there is remarkable alignment in one direction which is one of the three ⟨100⟩ directions. In fact, the alignment was evident over the entire grain (several hundred micrometres). Surprisingly (under no external stress), the material has globally picked only one of three crystallographically equivalent directions. This is exactly the behaviour predicted by our theory in Regime II.

4. Conclusion

As demonstrated above, the proof of theorem 3.5 relies on $\hat{W}$ possessing the properties (A1)–(A3) of remark 3.3. In particular, (A2), stating the strict convexity of $\hat{W}(\chi,\cdot)$, is problematic, because in space dimensions $D>1$, $\hat{W}$ is only quasi-convex. Thus, at present, further assumptions, i.e. $\partial_\varepsilon \beta^*(\chi,\varepsilon)=0$ in theorem 3.2, are needed to ensure the existence of weak solutions. These assumptions rule out local changes of the regime. (However, the available visual experimental evidence appears to indicate that the system is globally in a single regime at any given time.)

A further drawback is that the verification of (A1)–(A3) relies on (lengthy) explicit expressions for $\hat{W}$, $\partial_\chi \hat{W}$ and $\partial_\varepsilon \hat{W}$ which change with dimension and are not yet known in full generality in three dimensions. What is needed is a strategy of proof that requires only quasi-convexity of $\hat{W}$ and uses only its abstract properties as opposed to explicit expressions.

Another open question is the extension of theorem 3.4 to $\alpha_1 \neq \alpha_2$. The current proof fails in this case because it seems impossible to control the term

$$\int_{\Omega\times(0,t_0)} (\partial_\chi \hat{W}(\chi^B,\varepsilon^B)-\partial_\chi \hat{W}(\chi^B,\varepsilon^A))(\chi^B-\chi^A)\,\mathrm{d}x\,\mathrm{d}t,$$

with (χ^A,ε^A), (χ^B,ε^B) denoting two pairs of solutions.

As noted in §2*b*, there is clear experimental evidence that coarsening obeys a one-third power law, even in the presence of elastic effects, provided the interfacial area density is used as a measure of particle size. Whether this is indeed the case for the system presented here needs to be investigated.

Finally, another objective is the incorporation of plasticity in our model. Our two-scale approach allows the use of different approaches on the macro- and the microscale including phenomenological corrections to the energy on either scale.

Acknowledgement. Section 3*f* builds on [21] and benefited from discussions with Kaushik Bhattacharya.

Funding statement. T.B. acknowledges support by the German Science Foundation (DFG) under grant BL 512 4/1. I.V.C. thanks the Max Planck Institute for Mathematics in the Sciences, Leipzig for hospitality during a visit.

References

1. Voorhees PW. 1992 Ostwald ripening of two-phase mixtures. *Annu. Rev. Mater. Sci.* **22**, 197–215. (doi:10.1146/annurev.ms.22.080192.001213)
2. Fratzl P, Penrose O, Lebowitz JL. 1999 Modeling of phase separation in alloys with coherent elastic misfit. *J. Statist. Phys.* **95**, 1429–1503. (doi:10.1023/A:1004587425006)
3. Baldan A. 2002 Progress in Ostwald ripening theories and their applications to nickel-base superalloys. Part I. Ostwald ripening theories. *J. Mater. Sci.* **37**, 2171–2202. (doi:10.1023/A:1015388912729)
4. Baldan A. 2002 Progress in Ostwald ripening theories and their applications to the gamma′-precipitates in nickel-base superalloys. Part II. Nickel-base superalloys. *J. Mater. Sci.* **37**, 2379–2405. (doi:10.1023/A:1015408116016)

5. Ratke L, Voorhees PW. 2002 *Growth and coarsening: Ostwald ripening in material processing. Engineering materials*. Berlin, Germany: Springer.
6. Blesgen T, Chenchiah IV. 2011 A generalized Cahn–Hilliard equation incorporating geometrically linear elasticity. *Interfaces and Free Boundaries* **13**, 1–27. (doi:10.4171/IFB/246)
7. Novick-Cohen A. 2008 The Cahn–Hilliard equation. In *Handbook of differential equations: evolutionary equations* (eds CM Dafermos, M Pokorny), pp. 201–228. Amsterdam, the Netherlands: Elsevier.
8. Socrate S, Parks DM. 1993 Numerical determination of the elastic driving force for directional coarsening in Ni-superalloys. *Acta Metall. Mater.* **41**, 2185–2209. (doi:10.1016/0956-7151(93)90389-A)
9. Su CH, Voorhees PW. 1996 The dynamics of precipitate evolution in elastically stressed solids. I. Inverse coarsening. *Acta Mater.* **44**, 1987–1999. (doi:10.1016/1359-6454(95)00284-7)
10. Su CH, Voorhees PW. 1996 The dynamics of precipitate evolution in elastically stressed solids. II. Particle alignment. *Acta Mater.* **44**, 2001–2016. (doi:10.1016/1359-6454(95)00285-5)
11. Jou HJ, Leo PH, Lowengrub JS. 1997 Microstructural evolution in inhomogeneous elastic media. *J. Comput. Phys.* **131**, 109–148. (doi:10.1006/jcph.1996.5581)
12. Leo PH, Lowengrub JS, Nie Q. 2000 Microstructural evolution in orthotropic elastic media. *J. Comput. Phys.* **157**, 44–88. (doi:10.1006/jcph.1999.6359)
13. Zhu J, Chen LQ, Shen J. 2001 Morphological evolution during phase separation and coarsening with strong inhomogeneous elasticity. *Model. Simul. Mater. Sci. Eng.* **9**, 499–511. (doi:10.1088/0965-0393/9/6/303)
14. Akaiwa N, Thornton K, Voorhees PW. 2001 Large-scale simulations of microstructural evolution in elastically stressed solids. *J. Comput. Phys.* **173**, 61–86. (doi:10.1006/jcph.2001.6842)
15. Thornton K, Akaiwa N, Voorhees PW. 2004 Large-scale simulations of Ostwald ripening in elastically stressed solids: I. Development of microstructure. *Acta Mater.* **52**, 1353–1364. (doi:10.1016/j.actamat.2003.11.037)
16. Thornton K, Akaiwa N, Voorhees PW. 2004 Large-scale simulations of Ostwald ripening in elastically stressed solids. II. Coarsening kinetics and particle size distribution. *Acta Mater.* **52**, 1365–1378. (doi:10.1016/j.actamat.2003.11.036)
17. Zhu JZ, Wang T, Ardell AJ, Zhou SH, Liu ZK, Chen LQ. 2004 Three-dimensional phase-field simulations of coarsening kinetics of gamma′ particles in binary Ni–Al alloys. *Acta Mater.* **52**, 2837–2845. (doi:10.1016/j.actamat.2004.02.032)
18. Garcke H, Weikard U. 2005 Numerical approximation of the Cahn–Larché equation. *Numer. Math.* **100**, 639–662. (doi:10.1007/s00211-004-0578-x)
19. Prikhodko SV, Ardell AJ. 2003 Coarsening of gamma′ in Ni-Al alloys aged under uniaxial compression. III. Characterization of the morphology. *Acta Mater.* **51**, 5021–5036. (doi:10.1016/S1359-6454(03)00328-8)
20. Pollock TM, Argon AS. 1994 Directional coarsening in nickel-base single crystals with high volume fractions of coherent precipitates. *Acta Metall. Mater.* **42**, 1859–1874. (doi:10.1016/0956-7151(94)90011-6)
21. Chenchiah IV. 2004 *Energy-minimizing microstructures in multiphase elastic solids*. California Institute of Technology.
22. Valles JL, Arrell DJ. 1994 Monte Carlo simulation of anisotropic coarsening in nickel-base superalloys. *Acta Metall. Mater.* **42**, 2999–3008. (doi:10.1016/0956-7151(94)90396-4)
23. Nabarro FRN, Cress CM, Kotschy P. 1996 The thermodynamic driving force for rafting in superalloys. *Acta Mater.* **44**, 3189–3198. (doi:10.1016/1359-6454(95)00423-8)
24. Veron M, Brechet Y, Louchet F. 1996 Directional coarsening of Ni-based superalloys: Computer simulation at the mesoscopic level. *Acta Mater.* **44**, 3633–3641. (doi:10.1016/1359-6454(96)00011-0)
25. Paris O, Fährmann M, Fährmann E, Pollock TM, Fratzl P. 1997 Early stages of precipitate rafting in a single crystal Ni–Al–Mo model alloy investigated by small-angle X-ray scattering and TEM. *Acta Mater.* **45**, 1085–1097. (doi:10.1016/S1359-6454(96)00223-6)
26. Lund AC, Voorhees PW. 2003 A quantitative assessment of the three-dimensional microstructure of a gamma-gamma′ alloy. *Phil. Mag.* **83**, 1719–1733. (doi:10.1080/14786430310000080726)
27. Prikhodko SV, Ardell AJ. 2003 Coarsening of gamma′ in Ni–Al alloys aged under uniaxial compression: I. Early-stage kinetics. *Acta Mater.* **51**, 5001–5012. (doi:10.1016/S1359-6454(03)00329-X)

28. Ardell AJ, Prikhodko SV. 2003 Coarsening of gamma′ in Ni–Al alloys aged under uniaxial compression. II. Diffusion under stress and retardation of coarsening kinetics. *Acta Mater.* **51**, 5013–5019. (doi:10.1016/S1359-6454(03)00327-6)
29. Lund AC, Voorhees PW. 2002 The effects of elastic stress on coarsening in the Ni-Al system. *Acta Mater.* **50**, 2085–2098. (doi:10.1016/S1359-6454(02)00052-6)
30. Cahn JW, Hilliard JE. 1958 Free energy of a nonuniform system. I. Interfacial free energy. *J. Chem. Phys.* **28**, 258–267. (doi:10.1063/1.1744102)
31. Elliott CM. 1989 The Cahn-Hilliard model for the kinetics of phase separation. In *Mathematical models for phase change problems* (ed. JF Rodriques), pp. 35–54. Basel, Switzerland: Birkhäuser.
32. Elliott CM, Luckhaus S. 1991 *A generalized diffusion equation for phase separation of a multi-component mixture with interfacial free energy*, vol. 887, pp. 1–39. University of Minnesota Preprint. Q1
33. Alt HW, Pawłow I. 1992 A mathematical model of dynamics of nonisothermal phase separation. *Physica D: Nonlinear Phenom.* **59**, 389–416. (doi:10.1016/0167-2789(92)90078-2)
34. Alt HW, Pawłow I. 1996 On the entropy principle of phase transition models with a conserved order parameter. *Adv. Math. Sci. Appl.* **6**, 291–376.
35. Cahn JW, Elliott CM, Novick-Cohen A. 1996 The Cahn–Hilliard equation with a concentration dependent mobility: motion by minus the Laplacian of the mean curvature. *Eur. J. Appl. Math.* **7**, 287–3015. (doi:10.1017/S0956792500002369)
36. Watson SJ. 2004 Crystal Growth, coarsening and the convective Cahn—Hilliard equation. In *Free boundary problems* (eds P Colli, C Verdi, A Visintin), pp. 329–341. Basel, Switzerland: Birkhäuser.
37. Larché FC, Cahn JW. 1985 The interactions of composition and stress in crystalline solids. *Acta Metall.* **33**, 331–357. (doi:10.1016/0001-6160(85)90077-X)
38. Novick-Cohen A. 1988 On the viscous Cahn–Hilliard equation. *Material instabilities in continuum mechanics and related mathematical problems*. Oxford, UK: Clarendon Press.
39. Blesgen T. 1999 A generalization of the Navier–Stokes equations to two-phase flows. *J. Phys. D: Appl. Phys.* **32**, 1119–1123. (doi:10.1088/0022-3727/32/10/307)
40. Gurtin ME. 1996 Generalized Ginzburg–Landau and Cahn–Hilliard equations based on a microforce balance. *Physica D: Nonlinear Phenom.* **92**, 178–192. (doi:10.1016/0167-2789(95)00173-5)
41. Cahn JW, Novick-Cohen A. 1996 Limiting motion for an Allen–Cahn/Cahn–Hilliard system. In *Free Boundary Problems, Theory and Applications: Proceedings of the Zakopane Conference '95*, pp. 89–97. London, UK: Chapman and Hall/CRC.
42. Baldo S, Bellettini G. 1991 Gamma-convergence and numerical analysis: An application to the minimal partition problem. *Ric. Mat.* **40**, 33–64.
43. Sternberg P. 1991 Vector-valued local minimizers of nonconvex variational problems. *Rocky Mountain J. Math.* **21**, 799–807. (doi:10.1216/rmjm/1181072968)
44. Ambrosio L. 1990 Metric space valued functions of bounded variation. *Ann. Scuola Norm. Sup. Pisa Classe Sci. Ser. IV* **17**, 439–478.
45. Luckhaus S. 1991 The Stefan problem with Gibbs–Thomson law. *Sezione di Analisis Math. Prob. Univ. Pisa*. Q2
46. Cook HE. 1970 Brownian motion in spinodal decomposition. *Acta Metall.* **18**, 297–306. (doi:10.1016/0001-6160(70)90144-6)
47. Brassesco S, De Masi A, Presutti E. 1995 Brownian fluctuations of the interface in the $D=1$ Ginzburg–Landau equation with noise. *Ann. Inst. Henri Poincare Probab. Statist.* **31**, 81–118.
48. Garcke H, Rumpf M, Weikard U. 2001 The Cahn–Hilliard equation with elasticity: finite element approximation and qualitative studies. *Interfaces and Free Boundaries* **3**, 101–118. (doi:10.4171/IFB/34)
49. Garcke H. 2000 *On mathematical models for phase separation in elastically stressed solids*. Bonn, Germany: University of Bonn.
50. Garcke H. 2003 On Cahn–Hilliard systems with elasticity. *Proc. R. Soc. Edinburgh A: Mathematics* **133**, 307–331.
51. Garcke H. 2005 On a Cahn–Hilliard model for phase separation with elastic misfit. *Ann. Inst. Henri Poincare Anal. Nonlineaire* **22**, 165–185. (doi:10.1016/j.anihpc.2004.07.001)
52. Kay D, Welford R. 2006 A multigrid finite element solver for the Cahn–Hilliard equation. *J. Comput. Phys.* **212**, 288–304. (doi:10.1016/j.jcp.2005.07.004)
53. Chenchiah IV, Bhattacharya K. 2008 The relaxation of two-well energies with possibly unequal moduli. *Arch. Rat. Mech. Anal.* **187**, 409–479. (doi:10.1007/s00205-007-0075-3)

54. Larché FC, Cahn JW. 1982 The effect of self-stress on diffusion in solids. *Acta Metall.* **30**, 1835–1845. (doi:10.1016/0001-6160(82)90023-2)
55. Onsager L. 1931 Reciprocal relations in irreversible processes. I. *Phys. Rev.* **37**, 405–426. (doi:10.1103/PhysRev.37.405)
56. Onsager L. 1931 Reciprocal relations in irreversible processes. II. *Phys. Rev.* **38**, 2265–2279. (doi:10.1103/PhysRev.38.2265)
57. Dacorogna B. 2007 *Direct methods in the calculus of variations*, 2nd edn. Applied Mathematical Sciences. Berlin, Germany: Springer.
58. Kohn RV, Vogelius M. 1987 Relaxation of a variational method for impedance computed tomography. *Commun. Pure Appl. Math.* **40**, 745–777. (doi:10.1002/cpa.3160400605)
59. Blesgen T, Weikard U. 2005 A sharp interface model for phase transitions in crystals with linear elasticity. *Math. Meth. Appl. Sci.* **28**, 59–76. (doi:10.1002/mma.549)